

Optically induced spin polarisation of the NV^- centre in diamond: role of electron-vibration interaction

N.B. Manson¹, L. Rogers¹, M.W. Doherty², L.C.L. Hollenberg²
¹*Laser Physics Centre, Research School of Physics and Engineering,
 Australian National University, Australian Capital Territory, Australia*
²*School of Physics, University of Melbourne, Victoria, Australia*
 (Dated: 5-11-2010)

The novel aspect of the centre (NV^-) in diamond is the high degree of spin polarisation achieved through optical illumination. In this paper it is shown that the spin polarisation occurs as a consequence of an electron-vibration interaction combined with spin-orbit interaction, and an electronic model involving these interactions is developed to account for the observed polarisation.

PACS numbers: 76.70.Hb; 71.70.Fk; 71.70.Ej; 76.30.Mi

INTRODUCTION

Optically induced spin polarisation of the negatively charged nitrogen-vacancy centre in diamond (NV^-) has been known for a considerable time but there has not been a satisfactory account of how it arises. This lack of explanation is of concern considering that spin polarisation is the key property that sets this centre apart from all other optically active centres in solids and has enabled diamonds to be used for many new exciting applications such as magnetic sensing [1–8], probing biological materials [9–11], and quantum information processing [12–16]. In this work a transition within the spin-polarising decay path is studied using uniaxial stress. The order of the intermediate states involved is established, but more significantly it is shown that there is electron-vibration interaction associated with the lower level. This interaction is also involved in the important decay to the ground state, and it is clear that electron-vibration interaction is the factor that has been overlooked in previous treatments of the optical pumping cycle. Electron-vibration interaction plays a vital role in giving rise to spin polarisation and by including it in a model of the centre we can account for the observed level of spin polarisation.

UNIAXIAL STRESS

The NV^- centre in diamond has trigonal symmetry (C_{3v}) and a zero-phonon line (ZPL) at 637 nm (1.945 eV) corresponding to a ${}^3A_2 - {}^3E$ transition that can be observed in absorption and emission [17]. An additional ZPL at 1042.6 nm (1.19 eV) has been observed for a ${}^1A_1 - {}^1E$ transition in emission [18]. These lines and their inter-relationship are studied in this work using uniaxial stress. The line at 637 nm is measured in excitation is split by applied uniaxial stress as shown in figure 1a. The magnitude of the splittings are in good correspondence with those obtained in absorption by Hamer and Davies [17]. When the laser is tuned to one of the peaks in the spectrum, only one set of equivalent NV^- orientations

is excited and the infra red spectrum can be measured for the same set of orientations as in figure 1b. As assignments for the visible features are already known, this selective excitation technique allows the infrared lines to be reliably assigned (one modification is required from that given previously [18]). The variation of line positions of the infra red transition can be more conveniently obtained by exciting using an intense green beam where all orientations are excited simultaneously. The variation with stress is shown in figure 1c and 1d.

The zero-phonon line splittings are nearly all linear, and the strength of the various interactions giving rise to the shifts and splittings can be determined. The ZPL corresponds to $A - E$ transitions at the trigonal sites, and the interaction for this situation has been treated previously and can be expressed as

$$\begin{aligned}
 H_s = & A_1(s_{xx} + s_{yy} + s_{zz}) + A_1^t(s_{yz} + s_{zx} + s_{xy}) \\
 & + E_X(s_{xx} + s_{yy} - 2s_{zz}) + E_Y\sqrt{3}(s_{xx} - s_{yy}) \\
 & + E_X^t(s_{yz} + s_{zx} - 2s_{xy}) + E_Y^t\sqrt{3}(s_{yz} - s_{zx}) \quad (1)
 \end{aligned}$$

where A_1 and E_X , E_Y , E_X^t , E_Y^t are electronic operators and s_{ij} are components of the stress tensor [17, 19]. The notation is that adopted by [17] except a suffix t is used rather than a dash to indicate the terms which arise from T_2 terms in T_d symmetry. The E_X , E_Y symmetry-related distortions are in the plane of the three carbons, whereas those associated with E_X^t , E_Y^t are out of the plane (figure 2). The shift of levels for the various stress directions have been given by [17] using parameters A_1 , A_2 , B and C associated with the interaction terms A_1 , A_1^t , E and E^t respectively. These splitting parameters for the infrared transitions are summarised in table I. The visible NV^- transition at 637 nm and the NV^0 transition at 575 nm also correspond to $A - E$ transitions and the values for these transitions are given for comparison.

There is one transition where the displacement with stress is not linear. This is the case for [110] stress where a line curves to higher energy with increasing stress. For the same situation a new line is observed at -115 cm^{-1} as shown in figure 3. The new line is displaced in the re-

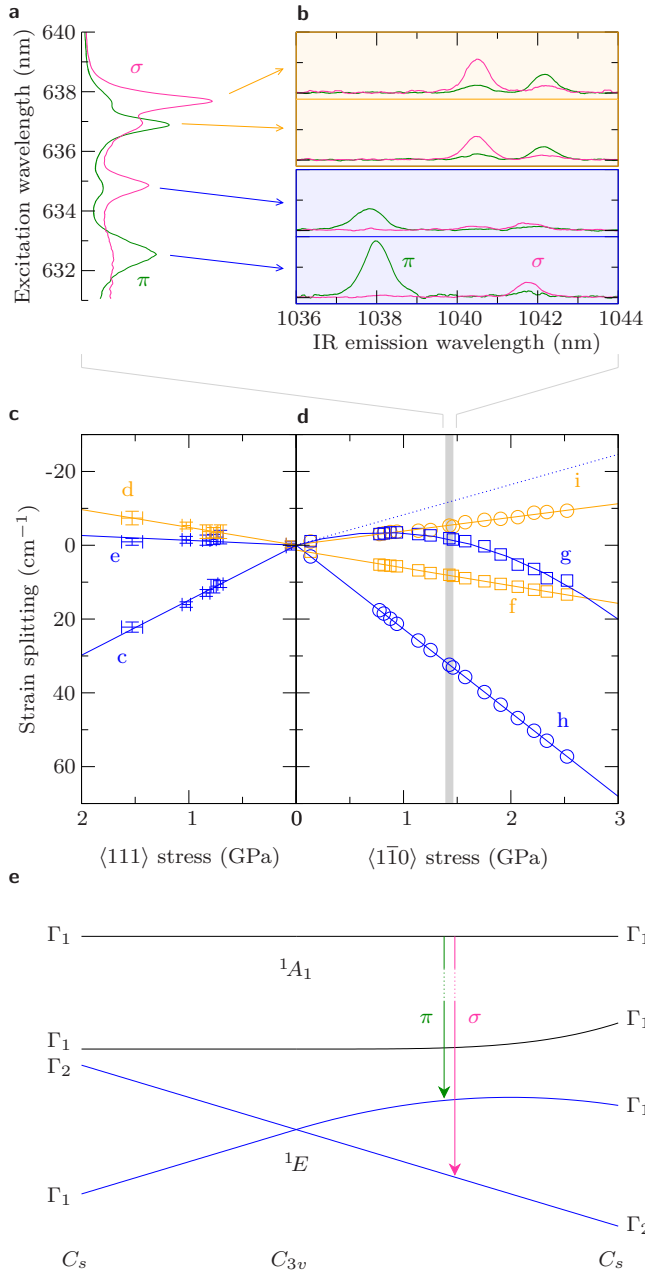


Figure 1: **ZPL splittings due to uniaxial stress.** **a**, The 637 nm visible ZPL measured in excitation. **b**, The corresponding IR photoluminescence spectra for resonant excitation on each visible peak. Resonantly exciting allowed selection of the multiple defect orientations. **c**, Strain splitting for the IR line for $\langle 111 \rangle$ stress. **d**, Strain splitting for the IR line for $\langle 1\bar{1}0 \rangle$ stress. **e**, Schematic diagram of the splitting and mixing levels involved in the IR transition.

verse sense and gains intensity at the expense of the former, indicating that the two levels are interacting. The line is on the low energy side of the emission spectrum, and so corresponds to a level either below the emitting level or above the lower level. The first option would lead to strong emission from the new level particularly once

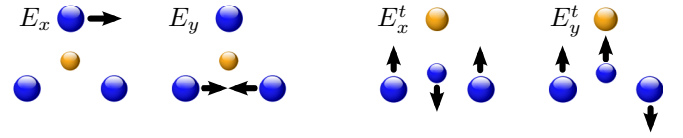


Figure 2: **Symmetry adapted distortions.** E_x and E_y are in the plane of the carbon atoms, while E_x^t and E_y^t are out of the plane.

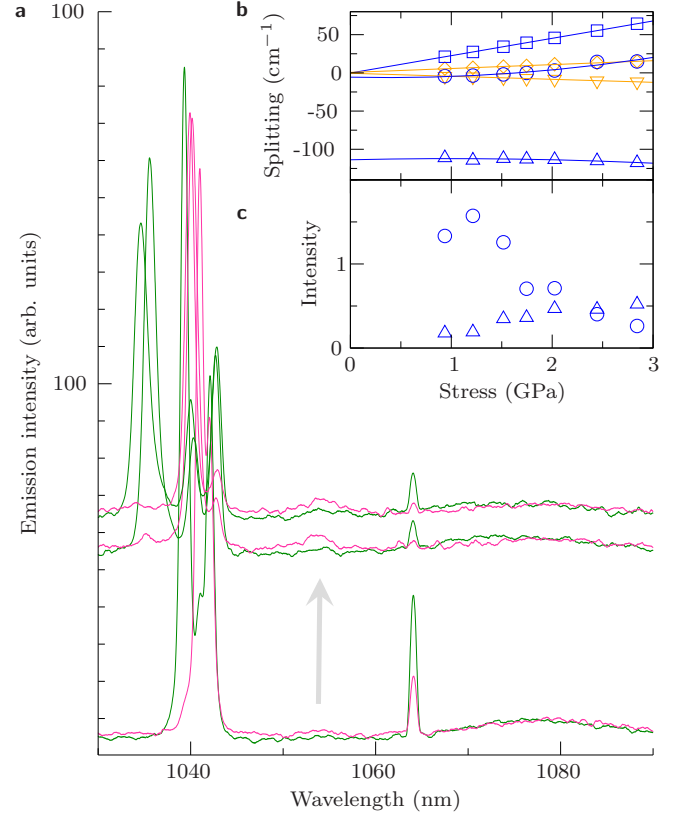


Figure 3: **New spectral line.** **a**, Emission spectra in π and σ polarisations for increasing applied stress, displaced vertically for clarity. The sharp feature at 1064 nm is due to laser scatter, and between it and the ZPL a broader weak feature is present at higher strains as indicated by the arrow. **b**, The splitting pattern from Figure 1d shown with the new line that appears at -115 cm⁻¹. **c**, The new line gains intensity at the expense of the nonlinear ZPL component.

the transition becomes allowed, which is not observed, and so the new level must be on the high energy side of the lower state. It only gains intensity as a consequence of mixing with one of the stress split components of the lower state, which must be the orbital E to split. This provides conclusive evidence that the 1E is the lower level and the 1A_1 the emitting level, resolving the recent contention surrounding the order of the levels involved in the infrared transition [18, 20–22].

For a $[110]$ stress orientation, a reflection plane is maintained resulting in C_s symmetry. A $\Gamma_1(E_x)$ component

of 1E is shifted up in energy and as there is interaction, the new state must likewise have Γ_1 symmetry. As there is no splitting the level will have A_1 symmetry in C_{3v} . There is no interaction when the stress is applied along the [001] direction as in this case a Γ_2 (E_Y) state is increased in energy and will not interact with a Γ_1 (illustrated in figure 1e). Note the reverse situation occurs for the NV^0 centre, with a new line and non-linear shifts for [111] (and [001]) stress being reported by Davies [23]. In that centre a linear shift is observed for a [110] stress and this is consistent with Davies' data points. The difference is due to the fact that the interacting level in the NV^0 case has A_2 symmetry.

Table I: Stress parameters of the NV^- and NV^0 ZPLs in $\text{cm}^{-1}/\text{GPa}$.

	NV^- 1042.6 nm	NV^- 637 nm	NV^0 575 nm
A_1	3.9	12.3	8.5
A_2	-3.05	-31.5	-28.6
B	9.85	7.96	12.5
C	5.59	14.26	14.1

The extra level at $\sim 115 \text{ cm}^{-1}$ for both the NV^- and NV^0 centres is attributed to the occurrence of a dynamic Jahn-Teller effect. The first vibronic state has $E \times E$ symmetry, which is split by linear electron-vibration interaction into $E + (A_1 + A_2)$ with the E displaced upward and $(A_1 + A_2)$ downward. The A_1 and A_2 degeneracy is lifted by quadratic interaction where the order depends on sign: A_1 lower for NV^- and A_2 lower for NV^0 . The interaction can involve a distribution of vibrations but when displaced down in energy to where there is a low density of vibrational states the feature becomes sharp. The 1A_1 transition from the emitting A_1 level to the A_1 vibronic state is allowed by group theory but has no oscillator strength and requires the mixing before the transition can be observed. The energy gap to the next higher vibronic state, A_2 , is too large to have sufficient mixing to be observed. The emission sideband at 344 cm^{-1} can be attributed to the upper E vibronic state shifted slightly up in energy. The size of the quadratic splitting is uncertain but indications are that there is pseudo-localised mode at 250 cm^{-1} and a Jahn-Teller energy of order of 200 cm^{-1} .

ELECTRONIC STRUCTURE

A full treatment of the electronic structure of the NV^- centre has been presented in a recent publication [24], whereas here we obtain insight by considering the centre as a trigonally distorted vacancy centre of six electrons in order to identify the correlations between the centre's different electronic states. In the trigonally distorted vacancy picture, the molecular orbitals (MOs) of

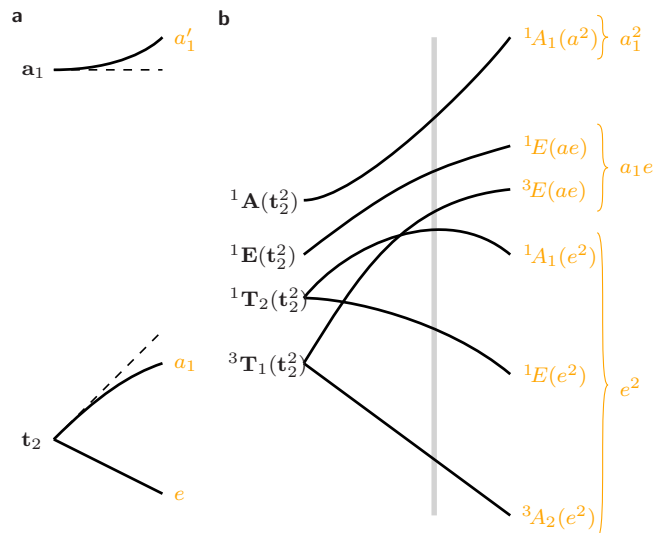


Figure 4: **Trigonal from tetrahedral.** **a**, Single-hole orbital energy scheme as t_d tetrahedral symmetry is distorted towards the C_{3v} trigonal limit. Tetrahedral symmetry labels are in bold, and the orange labels indicate the trigonal limit. **b**, Two-hole orbital energy scheme for the same distortion, where the shaded grey region indicates approximately the NV^- situation.

the centre are associated with the linear combinations of the dangling bonds in T_d point group symmetry, such that they transform as A_1 and T_2 and can be identified as \mathbf{a}_{1e} and \mathbf{t}_{2e} . The \mathbf{a}_{1e} is the lower energy MO, and so for six electrons, the lowest energy electronic configuration is $\mathbf{a}_{1e}^2 \mathbf{t}_{2e}^4$. This can be more conveniently described in terms of a two hole system, \mathbf{t}_2^2 . Lowering the symmetry from T_d to C_{3v} lifts the \mathbf{t}_2 degeneracy to give a two-fold degenerate $\mathbf{t}_{x,y} = e_{x,y}$ MO and a non-degenerate $\mathbf{t}_z = a_1$ MO. The e MO is independent of the strength of the trigonal field whereas the a_1 MO depends on the strength of the trigonal field as it is mixed with the higher energy a'_1 MO of the same symmetry associated with \mathbf{a}_1 (figure 4a). In the large trigonal field limit the two A_1 MOs (a_1 and a'_1) are related to the tetrahedral MOs as $a_1 = \sqrt{3}/2\mathbf{a}_1 + 1/2\mathbf{t}_z$ and $a'_1 = 1/2\mathbf{a}_1 - \sqrt{3}/2\mathbf{t}_z$.

Adopting the two-hole picture, the electronic configuration states generated by the different occupations of the hole MOs are depicted in figure 4 alongside their energies as functions of the hypothetical trigonal field. The energetic ordering of the states in both tetrahedral and strong trigonal field limits are taken to be consistent with Hund's rules. The \mathbf{t}_2^2 configuration gives rise to the configuration states ${}^3T_1(\mathbf{t}_2^2)$, ${}^1T_2(\mathbf{t}_2^2)$, ${}^1E(\mathbf{t}_2^2)$, and ${}^1A_1(\mathbf{t}_2^2)$. The ${}^3T_1(\mathbf{t}_2^2)$ state splits to give the lower ${}^3A_2(e^2)$ and the upper ${}^3E(ea_1)$ states in the trigonal field. The ground state ${}^3A_2(e^2)$ is independent of the size of the trigonal field, whereas the ${}^3E(ea_1)$ wavefunction varies with a_1 . It is known that there is a large nitrogen hyperfine interaction [25] and so a_1 has significant component of the

nitrogen dangling bond. The ${}^1\mathbf{T}_2(t_2^2)$ splits with the 1E decreasing in energy and the 1A_1 increasing in energy, but both interact with higher energy states of the same symmetry. In general, the states are admixtures ${}^1A_1 = {}^1A(e^2) + \kappa' A(a_1^2)$, ${}^1A_1' = {}^1A(a_1^2) - \kappa' {}^1A(e^2)$ and ${}^1E = {}^1E(e^2) + \kappa E(ea_1)$, ${}^1E' = {}^1E(ea_1) - \kappa {}^1E(e^2)$.

The presence of the ${}^1A_1 - {}^1E$ transition indicates the situation is far from the large trigonal limit, where it would have zero oscillator strength. In that limit the ZPL would not be displaced by A_1 stress components, but the nonzero A_1 and A_2 parameters indicate that it is in fact displaced. Furthermore, the ${}^1E \approx {}^1E(e^2)$ state would have exactly equal contribution of e_x and e_y MOs in the large trigonal field limit and would thus not split with E stress components, which is clearly inconsistent with the observed splitting (B and C parameters). From the magnitude of the stress parameters of the ${}^1A_1 - {}^1E$ transition, particularly in comparison to the ${}^3A_2 - {}^3E$ transition, an estimate can be made for κ to be of the order of 0.3. In the large trigonal field limit κ is zero, and $-i\ln T_d$ symmetry the 1E state can be re-expressed as ${}^1E = \sqrt{2/3} {}^1E(e^2) + \sqrt{1/3} {}^1E(ea_1)$ corresponding to a κ value of 0.7. Hence, the observed NV^- situation with $\kappa = 0.3$ is intermediary and is indicated by the vertical line in figure 4b.

Spin-orbit interaction can be included in the above model of the configuration states arising from the t_2^2 configuration by considering the variation of the transverse and axial spin-orbit parameters with the trigonal field. In the t_2^2 configuration, the spin-orbit interaction is given by

$$V_{so} = \Lambda_x S_x + \Lambda_y S_y + \Lambda_z S_z \quad (2)$$

where Λ_x and Λ_y are the transverse spin-orbit parameters, Λ_z is the axial spin-orbit parameter, and S_i are electronic spin operators for $i = x, y, z$. In T_d symmetry $\Lambda_x = \Lambda_y = \Lambda_z$, whereas in C_{3v} the $\Lambda_x = \Lambda_y \neq \Lambda_z$. Note that a detailed treatment of spin-orbit and spin-spin interactions was included in the recent publication [24]. The interactions give the fine structure and this is shown in the energy level schematic in figure 5. What is very important is that the triplet states are split into states either with $m_s = 0$ or with $m_s = \pm 1$ spin projection. There is one minor mixing which will be mentioned later. Optical transitions do not change spin projection and so the centre will remain in one of the spin projections after optical excitation. However, spin-orbit interaction will mix singlets with either of the triplet spin projections and a change of spin projection can result through intersystem crossings. An intersystem crossing will occur non-radiatively through interactions with vibrations, but the electron-vibration interaction can not by itself change spin projection. For this reason the energy levels of the NV^- centre are presented in figure 5 with the admixed components arranged in three columns for $m_s = 0$, $m_s = \pm 1$ and $S = 0$. The figure enables the allowed intersystem decay to be readily determined.

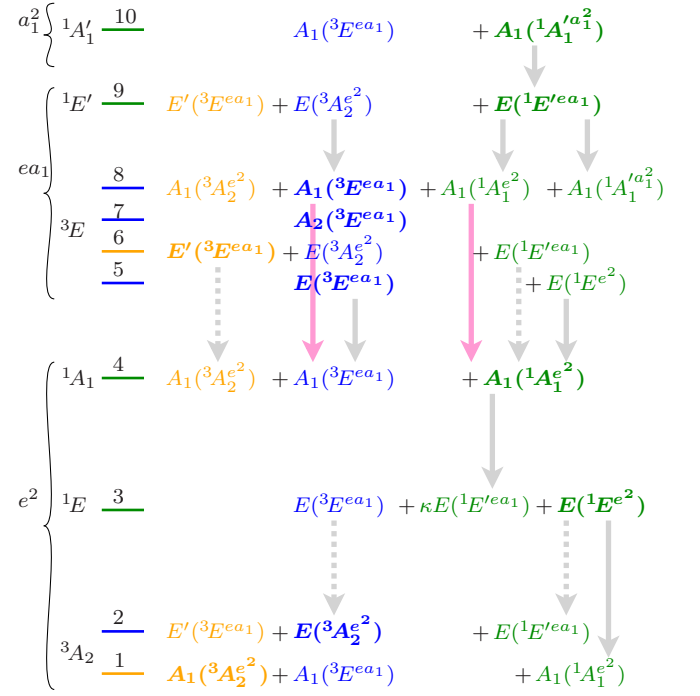


Figure 5: **Mixing between levels.** The first column (orange) contains $m_s = 0$ components, the second column (blue) contains $m_s = \pm 1$ components, and the final column (green) contains the $S = 0$ singlets. The primary two-hole configuration for each level is indicated in bold, and the other terms in ordinary typeface are admixed components. The coefficient κ draws attention to the mixing in the lower 1E level.

The most common situation is for the non-radiative decay to occur through A_1 vibrations. For this, the two states involved in the intersystem crossing have not only to be of the same irreducible representation but have to have an admixture of a common state. There is a further restriction in that the vibrational decay will be weak for large energy gaps requiring many vibrations and so only adjacent states are considered. By inspecting figure 5 it can be seen that the A_1 spin-orbit component of ${}^3E(ea_1)$ and the 1A_1 singlet level are intermixed and, therefore, allow decay via A_1 vibrations. For the same reason there can be decay from ${}^1E'$ to ${}^3E(ea_1)$ but the singlet is unlikely to be populated if above the triplet. There can be radiative decay to the 1E but there is no allowed decay path from the lowest singlet. The minimal decay in the upper levels and none returning the system to the ground state makes it clear that optically induced spin polarisation can not occur through spin-orbit interaction and A_1 vibrations alone.

ELECTRON-VIBRATION INTERACTION INDUCED INTERSYSTEM CROSSING

The factor not considered in the above is electron-vibration interaction. It is potentially a significant factor, as it can enable alternative non-radiative decay between states as will be discussed in this section, and dynamic effects within a state as discussed in the next section. A tetrahedron has symmetry adapted displacements with A_1 , E and T_2 symmetry giving $2A_1$ and $2E$ distortions in trigonal symmetry. The linear electron-vibration interaction associated with such symmetry adapted vibrations can be written in T_d as

$$H_{e-v} = V_{A_1} Q_{A_1} + V_{E_x} Q_{E_x} + V_{E_y} Q_{E_y} + V_{T_2x} Q_{T_2x} + V_{T_2y} Q_{T_2y} + V_{T_2z} Q_{T_2z} \quad (3)$$

and in C_{3v}

$$H_{e-v} = V_{A_1} Q_{A_1} + V_{E_x} Q_{E_x} + V_{E_y} Q_{E_y} + V_{E_z} Q_{E_z} + V_{E_y^t} Q_{E_y^t} + V_{A_1^t} Q_{A_1^t} \quad (4)$$

The additional decay channels introduced by electron-vibration interaction are those allowed by E -vibrations and can be determined from figure 5. These involve transitions where there is a change of the one electron orbits from a_1 to e or between the components of e (e_x to e_y). In the case of the lowest transition between the 1E and the 3A_2 ground state, decay is allowed to both of the ground state components as indicated in figure 5. The decay to the E ground state component ($m_s = \pm 1$) involves a change between a_1 and e orbits, whereas the decay to the A_1 component ($m_s = 0$) involves a change of the e orbits. As all the spin-orbit mixings are for well separated states they will be of similar magnitude and, therefore, the relative decay rates will depend on these different orbit changes. The electron orbits for both initial and final states lie largely on the three adjacent carbons and it is likely that the E -vibration involved in the intersystem crossing will be that involving the in-plane vibration of these atoms. The reduced matrix elements of electron-vibration interaction associated with this E vibration are related to the reduced matrix elements for tetrahedral symmetry, $\langle t_{x,y} || V_E || t_{x,y} \rangle$, $\langle t_z || V_E || t_{x,y} \rangle$ and $\langle a_1 || V_E || t_{x,y} \rangle$. The first two are equal whereas the third is zero as $T_2 \otimes E$ does not contain A_1 . In the large trigonal field limit, where a_1 is a linear combination of \mathbf{a}_1 and \mathbf{t}_z as given earlier, it is found that the reduced matrix element $\langle a_1 || V_E || e \rangle = \sqrt{1/4} \langle e || V_E || e \rangle$. It has been shown above that NV^- is not in the extreme trigonal field limit, but $\langle a_1 || V_E || e \rangle$ will be still smaller than $\langle e || V_E || e \rangle$ (estimate $1/\sqrt{3}$). From this it can be deduced that the reduced matrix elements associated with the transition to the A_1 component ($m_s = 0$) will be stronger than those to the E component $m_s = \pm 1$ of the ground state by a factor of $3/2$. Thus, the decay will favour the population of the $m_s = 0$ level of the ground state spin triplet.

The upper triplet-singlet ${}^3E - {}^1A_1$ inter-system crossing is also of great importance. As discussed above, relaxation from the A_1 spin-orbit component of 3E can decay to the singlet via A_1 -symmetry vibrations, but with electron-vibration interaction there are four additional decay channels from the E states allowed by E -vibrations. As the states involve ea_1 and e^2 configurations there is not the same justification for considering only one of the E -symmetry vibrations. The four decay channels are, however, not all equal as there will be a large variation in the magnitude of spin-orbit mixing. In particular two of these are large owing to the 1A_1 and ${}^1E'$ singlets undoubtedly lying adjacent to the 3E excited state triplet. The exact positions of the singlets are not yet known and so the relative strength of the two E -vibration induced relaxation and their strength relative to the A_1 -vibration induced relaxation cannot be estimated theoretically. However, the relative intersystem crossing rates can be obtained experimentally by comparing the emission responses upon switching on a pumping field for the cases where the system is unpolarised, polarised by previous optical excitation or inverted polarisation utilising a microwave π pulse. Such measurements have been given for ensembles [26] and single sites [27, 28]. The crossing rate for $m_s = \pm 1$ states are estimated to be factor of six times faster than that for $m_s = 0$ states [28]. This requires the decay involving A_1 vibrations to be slightly more than a factor of two faster than those involving E vibrations.

The electron-vibration interaction is also important for the decay between the singlets, ${}^1A_1 - {}^1E$. It does not require spin-orbit mixing and consequently can be a strong transition and is known to dominate over the radiative transition between these levels [18]. In this and other cases we have only discussed the decay in terms of the linear process implying only one E -vibration. However, this is the enabling process and other A_1 vibrations or pairs of E vibrations will be involved in compensating for the energy gap.

ELECTRON-VIBRATION INTERACTION WITHIN ELECTRONIC STATES

A degenerate vibration interacting with an orbitally degenerate electronic state can give rise to a Jahn-Teller or dynamic Jahn-Teller (DJT) effect and the uniaxial stress measurements showed that there was just such an effect in the lowest singlet state 1E . In the previous section it has been argued that there is spontaneous decay to the ground state via E vibrations. This does not require vibrations to be present in the lattice but there is the possibility of an additional process at higher temperatures when the lowest A_1 vibronic level is populated. From this A_1 state there can be decay to the ground state with the annihilation of the E vibration combined

with additional A_1 vibrations or pairs of E -vibrations to make up for the energy mismatch (anticipated to be of the order of 5000 cm^{-1}). The additional decay path will result in a temperature dependent 1E lifetime and this has been observed in both absorption [29] and emission recovery [28]. The two papers both reported a temperature dependence consistent with populating a level at 128 cm^{-1} (16 meV). The variance from the 115 cm^{-1} observed here will be due to their value corresponding to a distribution average and this one to a peak.

The presence of DJT is already known to occur in the excited 3E state [30]. The electron-vibration interaction results in a change of the polarisation of the sideband from that of the zero-phonon transition [30] and the interaction with the low frequency distribution of E -vibrations leads to a T^5 broadening of the zero-phonon line rather than a more normal T^7 dependence [30]. There will be some quenching of the spin-orbit splitting, but the degree is unclear as the magnitude of the intrinsic spin-orbit is not known.

Another important consequence of the DJT effect in the excited 3E state is that for a fixed spin it mixes the orbital components (no $m_s = 0$ and $m_s = \pm 1$ mixing). The E_x component of the electron-vibration interaction mixes the A_1 spin-orbit level with the E_x level and enables population in the E_x state to decay via A_1 vibrations, and also A_1 population to decay via E vibrations. There is a similar situation for the E_y component of the interaction involving the E_y state. Note also that population in the A_2 state can decay because of such mixing. The consequence is that even at zero temperature the DJT will enhance the overall decay rates.

As temperature is increased there can be a real transfer of population between the 3E levels through a two E vibration process. The rate can become higher than the separation of the levels. This quenches orbital angular momentum and the result is that the excited 3E state behaves as an effective orbital singlet (figure 6). There are three spin projections in the ground and three in the excited state but in each case the $m_s = \pm 1$ states can be treated as one. The decay rate between the singlets is fast and so they can be treated as one level. Thus the dynamics of the centre can be modeled using 5 levels, and this is frequently the electronic model used in discussing room temperature observations [26, 28, 31].

RATE EQUATIONS FOR SPIN POLARISATION

The 5-level system is indicated in figure 6. The effective triplet-singlet intersystem crossing rates are the sum for the various 3E spin-orbit components, and are denoted by γ and γ' for transfer from $m_s = \pm 1$ and $m_s = 0$ respectively. The lower crossings are denoted by β and β' . Anticipating spin polarisation the dashed parameters are expected to be slower than the non-dashed paramete-

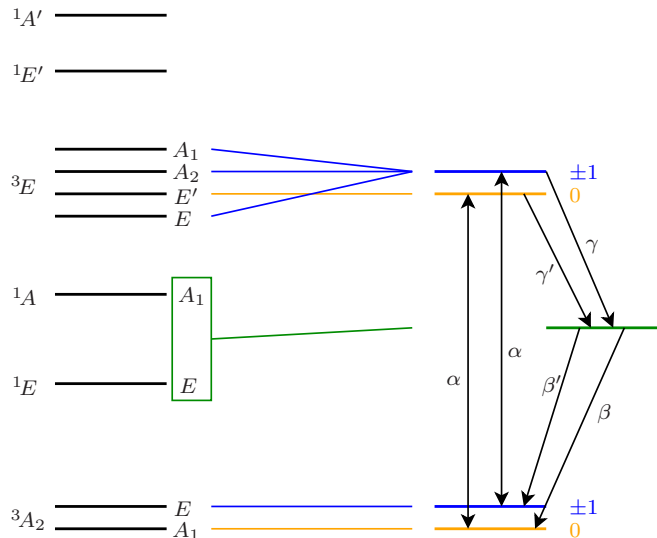


Figure 6: **Rate equation model.** At room temperature the NV⁻ system may be approximated as a 5-level model.

ters. The optical transition strength is taken as α . The model does not include a small mixing between the E and E' spin-orbit components of 3E state by spin-spin interaction. It is less than 1 percent and can be neglected for the case where the spin polarisation is not greater than 90 per cent. Assuming that the spin lattice relaxation is indefinitely long then the degree of spin polarisation is independent of the strength of the optical field. The population ratios in the excited state and ground states during continuous optical pumping are given by

$$\frac{P_{\pm 1}^e}{P_0^e} = \frac{\gamma' \beta'}{\gamma \beta} \quad (5)$$

$$\frac{P_{\pm 1}^g}{P_0^g} = \frac{\alpha + \gamma}{\alpha + \gamma'} \frac{\gamma' \beta'}{\gamma \beta} \quad (6)$$

Due to the faster intersystem crossing for $m_s = \pm 1$ states, there is always a smaller ratio (higher spin polarisation) in the excited state. $(\alpha + \gamma)/(\alpha + \gamma')$ is the ratio of the lifetimes $12.0\text{ ns}/7.8\text{ ns} = 1.54$ [32]. Different values will be obtained when the optical pumping is stopped. The polarisation will immediately reduce but by what amount depends on the β'/β ratio. Should high pump powers be used, so that prior to turning off the pump the majority of the population is in the singlet states, then after relaxation the polarisation will be determined largely by the β'/β ratio. Our above estimates suggest that this ratio is not very supportive of spin polarisation and it would be better to use low intensities. However, it does also indicate an opportunity to measure this ratio by examining spin polarisation as a function of the strength of the preparation pulse.

The intersystem crossing ratio to the ground state was estimated as $\beta'/\beta = 2/3$ and the upper crossing given earlier gives $\gamma'/\gamma = 1/6$. Consequently $(\gamma'/\gamma)(\beta'/\beta) =$

$2/18 = 0.11$ and for a lifetime ratio of $1/6$ corresponds to a ground state ratio of 0.18 . This indicates a ground state spin polarisation of 82 percent in the $m_s = 0$ state. This makes plausible comparison with experimental values of spin polarisation as they are also of the order of 80 per cent [15, 16, 28, 33]. Higher spin polarisation values would mean that the ratio β'/β is much smaller than our estimate. This would be the case should the reduced matrix element $\langle a_1 || V_E || e \rangle$ for the participating E vibration be very small but better estimates will require much more advanced theoretical modeling. However, it would be better to first establish the β'/β ratio experimentally.

DISCUSSION AND CONCLUSIONS

It should be recognised that due to the nature of spin-orbit interaction, intersystem crossings will always be spin selective and, hence, one can expect optical induced spin polarisation for all systems with $S \geq 1$ ground states. Whether this is observed depends on other factors. Obviously the centre needs to be stable and spin lattice relaxation times reasonably long. The important aspect highlighted by the present work is the rate and sign of the intersystem crossing. There will be two crossings, and for significant spin polarisation it is beneficial to have a high branching ratio between the alternative spin projections for the two crossings to favour the same spin. The rates will be faster if the levels are close and this is more readily achieved if there are two intermediate levels (such as the two singlets in the case of NV^-). An aspect not treated above is that optical spin readout requires the upper inter-system rate to be comparable to the optical rate, and this is probably only achievable if the levels are close to one phonon energy.

Clearly NV satisfies all of the above, but it should be realised that this is only achieved as a consequence of electron-vibration interaction. The upper intersystem crossing is between two close levels and although a reasonable rate maybe achievable without the vibration interaction the rate is certainly enhanced with vibrations. The vibration interaction enables additional decay paths and also improves the situation with mixing within the manifold through the DJT effect. The situation is more important for the lower intersystem crossing where without the electron-vibration interaction the lower singlet level would be metastable and population would simply be transferred from triplet to singlet. This is probably what happens in several other colour centres in diamond where the alternate spin state is sufficiently long lived, for example, to allow CW EPR measurements [34]. The interaction involves low frequency vibration and the specifics of the vibration are important as it can influence the rates for the different spins. It will not be a simple procedure to identify another ‘NV situation’. It may be easy to have equivalent energy structures even in similar

lattices, but it is hard to anticipate how to obtain appropriate strength of electron-vibration interaction and appropriate local vibrations.

The main point of the paper has been to show that optically induced spin polarisation can only be explained when the effect of electron-vibration interaction is included alongside the electronic spin-orbit interaction in the dynamics of the centre. By using the current electronic model and including simple considerations of electron-vibration interaction it is shown that the estimated spin polarisation is in agreement with experiment.

This work was supported by the Australian Research Council under the Discovery Project scheme DP0986635 and DPxxxxxxx.

-
- [1] B. M. Chernobrod and G. P. Berman, “Spin microscope based on optically detected magnetic resonance,” *Journal of Applied Physics*, vol. 97, no. 1, p. 014903, 2005.
 - [2] C. L. Degen, “Scanning magnetic field microscope with a diamond single-spin sensor,” *Appl. Phys. Lett.*, vol. 92, p. 243111, 2008.
 - [3] J. M. Taylor, P. Cappellaro, L. Childress, L. Jiang, D. Budker, P. R. Hemmer, A. Yacoby, R. Walsworth, and M. D. Lukin, “High-sensitivity diamond magnetometer with nanoscale resolution,” *Nature Physics*, vol. 4, pp. 810 – 816, 2008.
 - [4] J. R. Maze, P. L. Stanwix, J. S. Hodges, S. Hong, J. M. Taylor, P. Cappellaro, L. Jiang, M. V. G. Dutt, E. Togan, A. S. Zibrov, A. Yacoby, R. L. Walsworth, and M. D. Lukin, “Nanoscale magnetic sensing with an individual electronic spin in diamond,” *Nature*, vol. 455, pp. 644 – 647, 2008.
 - [5] G. Balasubramanian, I. Y. Chan, R. Kolesov, M. Al-Hmoud, J. Tisler, C. Shin, C. Kim, A. Wojcik, P. R. Hemmer, A. Krueger, T. Hanke, A. Leitenstorfer, R. Bratschkitsch, F. Jelezko, and J. Wrachtrup, “Nanoscale imaging magnetometry with diamond spins under ambient conditions,” *Nature*, vol. 455, pp. 648 – 651, 2008.
 - [6] L. T. Hall, J. H. Cole, C. D. Hill, and L. C. L. Hollenberg, “Sensing of fluctuating nanoscale magnetic fields using Nitrogen-Vacancy centers in diamond,” *Physical Review Letters*, vol. 103, p. 220802, Nov. 2009.
 - [7] J. H. Cole and L. C. L. Hollenberg, “Scanning quantum decoherence microscopy,” *Nanotechnology*, vol. 20, no. 49, p. 495401, 2009.
 - [8] L. T. Hall, C. D. Hill, J. H. Cole, B. Städler, F. Caruso, P. Mulvaney, J. Wrachtrup, and L. C. L. Hollenberg, “Monitoring ion-channel function in real time through quantum decoherence,” *Proceedings of the National Academy of Sciences*, vol. 107, pp. 18777 – 18782, Nov. 2010.
 - [9] C. Fu, H. Lee, K. Chen, T. Lim, H. Wu, P. Lin, P. Wei, P. Tsao, H. Chang, and W. Fann, “Characterization and application of single fluorescent nanodiamonds as cellular biomarkers,” *Proceedings of the National Academy of Sciences*, vol. 104, pp. 727 – 732, Jan. 2007.
 - [10] Y. Chang, H. Lee, K. Chen, C. Chang, D. Tsai, C. Fu, T. Lim, Y. Tzeng, C. Fang, C. Han, H. Chang, and

- W. Fann, “Mass production and dynamic imaging of fluorescent nanodiamonds,” *Nat. Nanotechnol.*, vol. 3, pp. 284–288, 2008.
- [11] J. Tisler, G. Balasubramanian, B. Naydenov, R. Kolesov, B. Grotz, R. Reuter, J. Boudou, P. A. Curmi, M. Sennour, A. Thorel, M. Börsch, K. Aulenbacher, R. Erdmann, P. R. Hemmer, F. Jelezko, and J. Wrachtrup, “Fluorescence and spin properties of defects in single digit nanodiamonds,” *ACS Nano*, vol. 3, pp. 1959–1965, July 2009.
- [12] T. Gaebel, M. Domhan, I. Popa, C. Wittmann, P. Neumann, F. Jelezko, J. R. Rabeau, N. Stavrias, A. D. Greentree, S. Prawer, J. Meijer, J. Twamley, P. R. Hemmer, and J. Wrachtrup, “Room-temperature coherent coupling of single spins in diamond,” *Nature Physics*, vol. 2, p. 408, June 2006.
- [13] M. V. G. Dutt, L. Childress, E. T. L. Jiang, J. Maze, F. Jelezko, A. S. Zibrov, P. R. Hemmer, and M. D. Lukin, “Quantum register based on individual electronic and nuclear spin qubits in diamond,” *Science*, vol. 316, pp. 1312–1316, June 2007.
- [14] E. Togan, Y. Chu, A. S. Trifonov, L. Jiang, J. Maze, L. Childress, M. V. G. Dutt, A. S. Sorensen, P. R. Hemmer, A. S. Zibrov, and M. D. Lukin, “Quantum entanglement between an optical photon and a solid-state spin qubit,” *Nature*, vol. 466, no. 7307, pp. 730–734, 2010.
- [15] P. Neumann, R. Kolesov, B. Naydenov, J. Beck, F. Rempp, M. Steiner, V. Jacques, G. Balasubramanian, M. L. Markham, D. J. Twitchen, S. Pezzagna, J. Meijer, J. Twamley, F. Jelezko, and J. Wrachtrup, “Quantum register based on coupled electron spins in a room-temperature solid,” *Nat Phys*, vol. 6, pp. 249–253, Apr. 2010.
- [16] G. D. Fuchs, V. V. Dobrovitski, D. M. Toyli, F. J. Hermans, C. D. Weis, T. Schenkel, and D. D. Awschalom, “Excited-state spin coherence of a single nitrogen-vacancy centre in diamond,” *Nat Phys*, vol. 6, no. 9, pp. 668–672, 2010.
- [17] G. Davies and M. F. Hamer, “Optical studies of the 1.945 eV vibronic band in diamond,” *Proc. R. Soc. Lond. A.*, vol. 348, pp. 285–298, 1976.
- [18] L. J. Rogers, S. Armstrong, M. J. Sellars, and N. B. Manson, “Infrared emission of the NV centre in diamond: Zeeman and uniaxial stress studies,” *New Journal of Physics*, vol. 10, no. 10, p. 103024, 2008.
- [19] A. E. Hughes and W. A. Runciman, “Uniaxial stress splitting of doubly degenerate states of tetragonal and trigonal centres in cubic crystals,” *Proc. Phys. Soc.*, vol. 90, pp. 827–838, 1967.
- [20] N. Manson and R. McMurtrie, “Issues concerning the nitrogen-vacancy center in diamond,” *Journal of Luminescence*, vol. 127, pp. 98–103, Nov. 2007.
- [21] A. Gali, M. Fyta, and E. Kaxiras, “Ab initio supercell calculations on nitrogen-vacancy center in diamond: Electronic structure and hyperfine tensors,” *Phys. Rev. B*, vol. 77, p. 155206, 2008.
- [22] P. Delaney, J. C. Greer, and J. A. Larsson, “Spin-Polarization mechanisms of the Nitrogen-Vacancy center in diamond,” *Nano Letters*, vol. 10, pp. 610–614, Feb. 2010.
- [23] G. Davies, “Dynamic Jahn-Teller distortions at trigonal optical centres in diamond,” *J. Phys. C*, vol. 12, no. 13, pp. 2551–2566, 1979.
- [24] M. W. Doherty, N. B. Manson, P. Delaney, and L. C. L. Hollenberg, “The negatively charged nitrogen-vacancy centre in diamond: the electronic solution,” *1008.5224*, Aug. 2010.
- [25] G. D. Fuchs, V. V. Dobrovitski, R. Hanson, A. Batra, C. D. Weis, T. Schenkel, and D. D. Awschalom, “Excited-state spectroscopy using single-spin manipulation in diamond,” *Phys. Rev. Lett.*, vol. 101, p. 117601, 2008.
- [26] N. B. Manson, J. P. Harrison, and M. J. Sellars, “Nitrogen-vacancy center in diamond: Model of the electronic structure and associated dynamics,” *Phys. Rev. B*, vol. 74, no. 10, p. 104303, 2006.
- [27] M. Steiner, P. Neumann, J. Beck, F. Jelezko, and J. Wrachtrup, “Universal enhancement of the optical readout fidelity of single electron spins at nitrogen-vacancy centers in diamond,” *Physical Review B*, vol. 81, p. 035205, Jan. 2010.
- [28] L. Robledo, H. Bernien, T. van der Sar, and R. Hanson, “Spin dynamics in the optical cycle of single nitrogen-vacancy centres in diamond,” *1010.1192*, Oct. 2010.
- [29] V. M. Acosta, A. Jarmola, E. Bauch, and D. Budker, “Optical properties of the nitrogen-vacancy singlet levels in diamond,” *1009.0032*, Aug. 2010.
- [30] K. C. Fu, C. Santori, P. E. Barclay, L. J. Rogers, N. B. Manson, and R. G. Beausoleil, “Observation of the dynamic Jahn-Teller effect in the excited states of Nitrogen-Vacancy centers in diamond,” *Physical Review Letters*, vol. 103, pp. 256404–4, Dec. 2009.
- [31] L. J. Rogers, R. L. McMurtrie, M. J. Sellars, and N. B. Manson, “Time-averaging within the excited state of the nitrogen-vacancy centre in diamond,” *New Journal of Physics*, vol. 11, no. 6, p. 063007, 2009.
- [32] A. Batalov, C. Zierl, T. Gaebel, P. Neumann, I. Chan, G. Balasubramanian, P. R. Hemmer, F. Jelezko, and J. Wrachtrup, “Temporal coherence of photons emitted by single Nitrogen-Vacancy defect centers in diamond using optical Rabi-Oscillations,” *Phys. Rev. Lett.*, vol. 100, no. 7, p. 077401, 2008.
- [33] J. Harrison, M. J. Sellars, and N. B. Manson, “Measurement of the optically induced spin polarisation of N-V centres in diamond,” *Diamond Relat. Mater.*, vol. 15, pp. 586–588, 2006.
- [34] S. Felton, A. M. Edmonds, M. E. Newton, P. M. Martineau, D. Fisher, and D. J. Twitchen, “Electron paramagnetic resonance studies of the neutral nitrogen vacancy in diamond,” *Physical Review B*, vol. 77, p. 081201, Feb. 2008.